Korean J. Chem. Eng., 36(2), 287-298 (2019)
DOI: 10.1007/s11814-018-0162-1

pISSN: 0256-1115
eISSN: 1975-7220

Ultrasound-assisted green synthesis and application of recyclable nanoporous chromium-based metal-organic framework

Niyaz Mohammad Mahmoodi†, Mohsen Taghizadeh, and Ali Taghizadeh

Department of Environmental Research, Institute for Color Science and Technology, Tehran, Iran
(*Received 10 July 2018 • accepted 8 October 2018*)

Abstract−We studied the synthesis, characterization clarification, and dye adsorption ability of chromium-based metal-organic framework (Materials Institute Lavoisier: MIL-101(Cr)). MIL-101(Cr) with 1 : 1 molar ratio of metal to ligand was ultrasound-assisted green synthesized in a DMF-free way and its adsorption capacity for pollutant remediation was studied. Several analyses were applied to clarify the characterization of materials, including TGA, SEM, XRD, FTIR, BET, and Zeta potential. Direct Red 80 (DR80) and Acid Blue 92 (AB92) were used to make model dye bearing wastewater. Response surface methodology (RSM) historical modeling was applied to the data to achieve an accurate model of the experiment. Adsorption kinetics and isotherms models were fully studied. The powerful adsorbent was the MIL-101(Cr) with the M/L=1 : 1, which represented the high specific surface area (SSA) of 2,420 m^2/g and surface charge of +27.2 mV. The maximum adsorption capacity was obtained 227 mg/g for DR80 and 185 mg/g for AB92. With an eye to the real-world application, the synthesized adsorbent well operated by removing dyes from the wastewater and high reusability after four cycles.

Keywords: Ultrasound-assisted Green Synthesis, High Specific Surface Area, MIL-101(Cr), Pollutant Remediation, RSM

INTRODUCTION

Water pollution has increased globally, and new worldwide methodologies have been applied for continued exploitation of water resources. Huge amounts of organic pollutants, especially dyes, are recognized to be one of the main causes of water contamination [1-7]. They are classified as non-biodegradable materials that stay intact under various conditions due to their synthetic base and sophisticated aromatic structures. They can aesthetically affect the environment and threaten the health of living organisms, such as human beings and other creatures [7-13]. Many different approaches for the purifying colored wastewater have been investigated [13-15]. Adsorption technique is considered as an effective way to rapidly lower the concentration of dissolved contaminants in waterways [16,17]. In addition, for requiring a relatively low operating temperature, this process can remove several pollutants and keep the wastewater volume to the smallest by transferring the contaminants from the aqueous phase to a solid phase [18-20]. The adsorption system developed by conventional adsorbents has provided researchers with ideas to study and design new materials capable of improving the process [21-23].

Recently, metal-organic frameworks (MOFs) were applied in the different fields such as solid-phase extraction, sensors, drug delivery, electronics, gas storage and antibacterial agents [24-32]. MOFs as solid crystalline and porous substances, which are synthesized by inorganic materials and organic ligands as connectors, have been applied in various industrial applications. Assembled on crystalline porous materials, the organic and inorganic substructures can bring about chemical adaptability that can provide many MOFs [33-37].

The unique features of MOFs, such as high specific surface area and high porous volume, which is quite a genuine parameter for surface absorption, make MOFs well adsorbent. For the recent decade, these materials were applied for removal of gaseous pollutants, air pollution elimination, and nowadays used to water and wastewater purification. The application of MOFs in water purification has gained momentum in the past five years [38]. Considering their interactions with the other materials, MOFs including open metal sites can show good performance and selectivity during the adsorption development [39-44]. As one of the known MOF materials with high potentials, MIL (Material Institute Lavoisier) has proven to be stable in water, acids or bases and high surface area MILs show higher stability in various solvents compared to other MOFs [45-47]. The $Cr_3O(F/OH)$ $(H_2O)_2[C_6H_4(CO_2)_2]$ known as MIL-101(Cr) is a porous chromium-benzene dicarboxylate (Cr-H_2BDCs) with an octahedral structure and a huge pore volume. The hybrid super tetrahedral serves as the basic building block of this hybrid solid, and consists of organic linkers and chromium III as octahedral clusters. Adsorptive removal of organic hazardous wastes from aqueous solution using MOFs has been the subject of extensive studies [47-50].

According to our best knowledge, so far, the dye removal ability of water-based synthesized MIL-101(Cr) has not been studied in detail. In the present study, MIL-101(Cr) with 1 : 1 metal to ligand ratio was green synthesized by ultrasound and used to remove DR80 and AB92, from colored wastewater. The SEM, TGA, XRD, FTIR, BET, and Zeta potential were performed and fully studied. Also, the influence of major variables on the adsorption process

†To whom correspondence should be addressed.
E-mail: mahmoodi@icrc.ac.ir, nm_mahmoodi@aut.ac.ir,
E-mail: nm_mahmoodi@yahoo.com

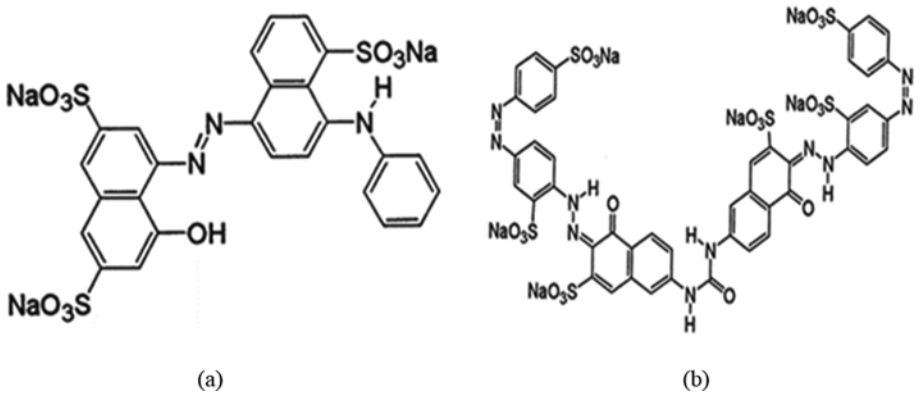

Fig. 1. The molecular structure of dyes (a) AB 92 (λ_{max}=571) and (b) DR 80 (λ_{max}=542.5).

was investigated and reported. To study dye removal rates and adsorption mechanisms, different isotherm and kinetic models were applied and all experimental data were used to achieve an accurate model using the RSM approach.

EXPERIMENTAL

1. Materials and Instruments

The DR80 and AB92 (Fig. 1) were purchased from Ciba Ltd. Chromium nitrate salt ($Cr(NO_3)_3{\cdot}9H_2O$) and ethanol (C_2H_6O) were obtained from Merck. Terephthalic acid 98% (H_2BDC) was from Sigma-Aldrich Company. In all the experiments, the solution pH was adjusted using NaOH and HCl solutions. Surface functional groups and morphological structure of the materials were studied by Perkin-Elmer spectrophotometer (Spectrum One) and SEM (LEO 1455VP), respectively. The crystal structure of materials was recognized by the XRD (model Siemens D-5000). The BET analyses were carried out by (BELSORP-mini II) through N_2 adsorption/desorption isotherms. The HORIBA (SZ-100, Japan) instrument was used to perform the zeta potential analysis [51].

2. MOFs Synthesis

The green synthesis approach was applied for synthesizing MIL-101(Cr) based on the metal to ligand ratio (Cr^{3+}: H_2BDC) [52]. H_2BDC: $Cr(NO_3)_3{\cdot}9H_2O$ with 1 : 1 molar ratios were sonicated in 10 ml of distilled water for 1 h then stirred for half an hour. A Teflon-lined autoclave was used to seal and heat the suspension at 218 °C for 18 h. Centrifuge filtration was used to separate the product. In the next stage, the products were rinsed three times with hot deionized water (373 K) and hot ethanol (333 K) before being dried at 393 K in a vacuum oven during the overnight.

3. Batch Adsorption Process

The dye adsorption potential of the synthesized MILs was tested by adsorption of DR80 and AB92 from aqueous solution. To optimize the involved effects on the adsorption condition, four main factors were investigated in a wide range. All tests were carried out at 298 K. A certain amount of MILs was added to dye solution (100 mL) with different concentrations (30-60 mg/L) in a wide range of pH to perform the dye adsorption process. The pH of solutions was fixed in acidic and basic range using HCl or NaOH. After that, the following formula was used to calculate the dye removal percentage:

$$R(\%) = (1 - C_0/C_t) \times 100 \quad (1)$$

The equilibrium concentration of adsorbate on the surface of MOFs was measured by [53]:

$$q_e = (C_0 - C_e/m) \times V \quad (2)$$

4. Statistical Methodology

RSM, as a great tool to get responses over all parameter space, combines the influences of all involved independent factors on the adsorption process. RSM is usually applied to design the experimental and modeling the response. In this research, experimental tests were done classically and the regression tool in free-trial of Design-Expert® 11 software, intended for RSM, was applied to historical data. In this study, the analyses of variance (ANOVA) of the data were carried out by considering the R^2. Over and above, the statistical value of the all model variables factor was measured by considering the probability value (P-value) and Fisher value (F-value).

RESULT AND DISCUSSION

1. Materials Characterization

Fig. 2 depicts the FTIR spectrum of the adsorbent. The peak value at 3,411.02 cm^{-1} obtained from MIL-101(Cr) is attributed to -OH stretch vibration of adsorbed moisture or the functional groups in a carboxylic acid (COOH) [54]. The broad peak located at 1,698.98 cm^{-1} belongs to the typical C=O stretch vibration of

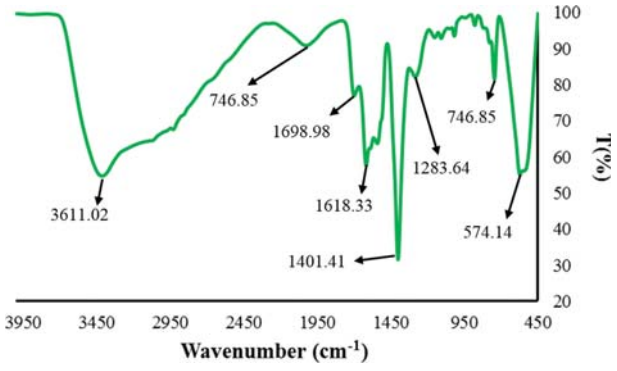

Fig. 2. The FTIR spectrum of the synthesized MIL-101(Cr).

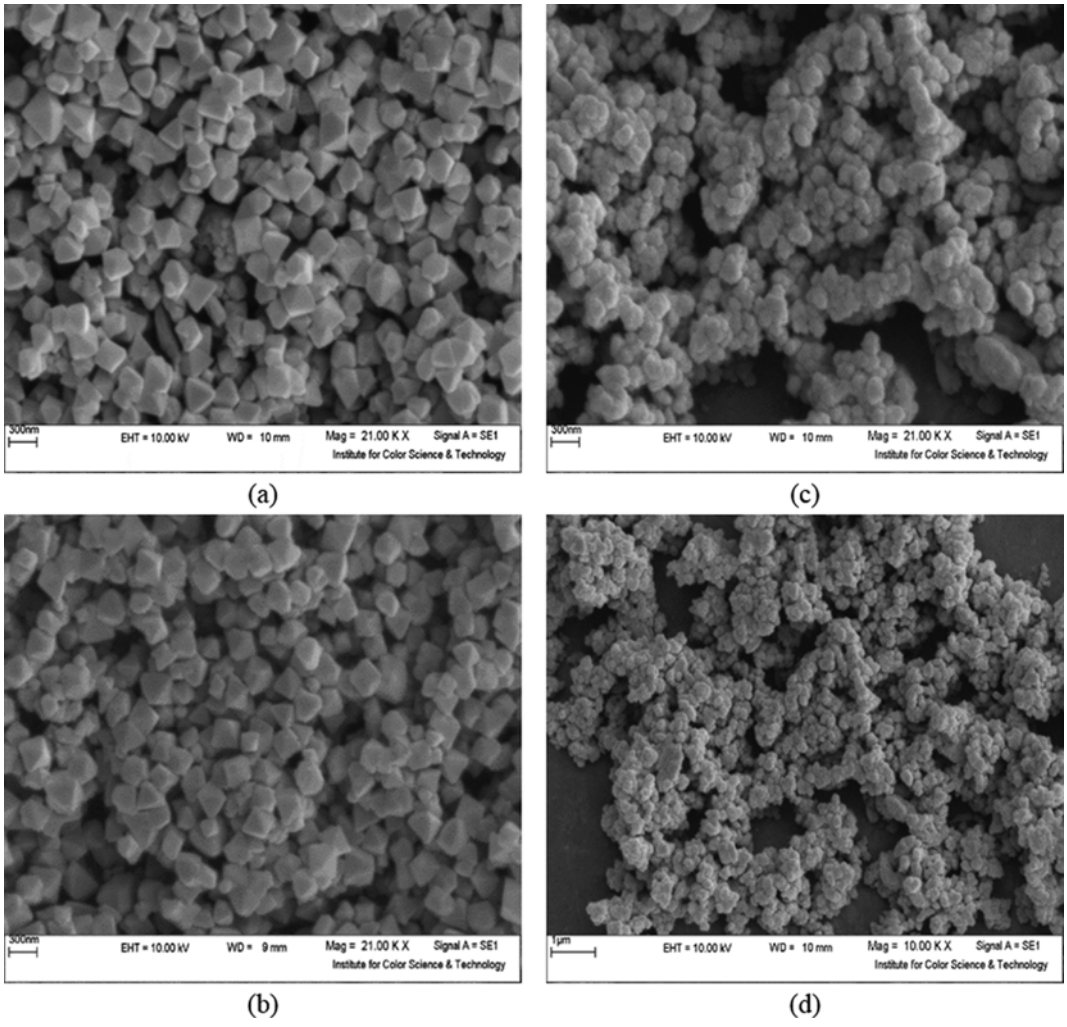

Fig. 3. SEM images of materials (a and b) MIL-101(Cr) and (c and d) 4th cycle of reused MIL.

framework's carboxylic acid. The peak at 1,618.33 cm^{-1} is mainly ascribed to the vibration of the aromatic ring in the benzene group which presented at linker structure [55]. The very strong sharp peak at 1,401.41 cm^{-1} is referred to the O-H bend vibration. The C-O stretch vibration of MOF can be seen at 1,283.64 cm^{-1}. The indicated peak at 746.85 cm^{-1} may be ascribed to the aromatic ring out-of-plane deformation vibrations. The considerable broad peak obtained from MOF at 574.14 cm^{-1} can cause by the =C-C-C existing in the plan bending of the aromatic benzene in the structure of dicarboxylic linkers.

The SEM images (Fig. 3) of the as-synthesized nanomaterial were presented to MIL morphology and particle size determination. According to the presented images, a homogeneous range of crystal size distribution (around 300 nm) was observed for MIL-101. As it can be seen from Fig. 3, the regenerated MOF particles after the 4th cycle reproducing became more irregular. This alteration is directly related to structural stability and shape transformation of MOF in aqueous solution. The SEM images show the uniform and smooth surface of an octahedral crystal of MIL with M/L 1 : 1. Although MILs-101 are considered as the most stable MOFs in the aqueous phase, the structural deformation of them is inevitable [38]. Despite this, the 4th cycle of reused MIL-101(Cr) shows the MOF retained its cubic symmetry shape of the crystals with little defor-

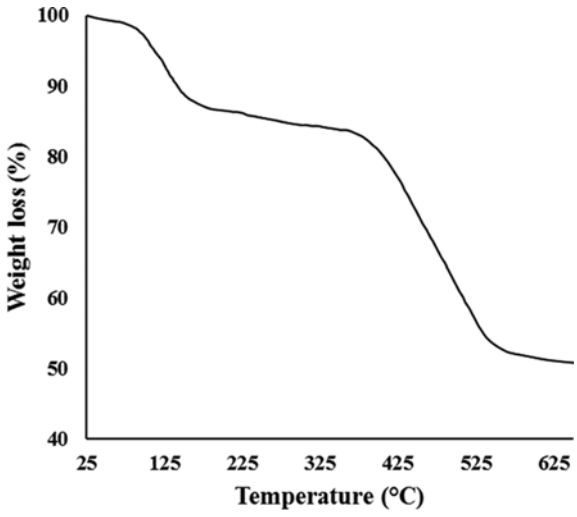

Fig. 4. TGA curve of the green synthesized MIL-101(Cr).

mation which related to the structural changes during the adsorption process [56].

To know the behavior of the adsorbent against the temperature changes, thermogravimetric analysis (TGA) of MIL was done (Fig. 4). According to the TGA thermograph of adsorbent, the MIL-101(Cr) weight change generally could be classified in two main stages. The first stage, initial weight loss, about 14% did occur in the range of 25 to 400 °C due to the release of adsorbed volatile materials [57,58]. According to the TGA graph data, from 400 °C to 530 °C, the second and major stage of weight change was observed. In this section, the quick drop on TGA curvature is attributed to the destruction of the adsorbent framework [59]. Actually, the second stage of weight loss is related to the complete degradation of benzenedicarboxylate linkers. Also, decomposition of chromium (III) oxide clusters occurs above 530 °C until reaching a constant percentage.

The present study is an attempt to precisely look into the crystalline structure of water-based synthesized MIL-101(Cr). Fig. 5 shows the XRD of MIL-101(Cr) before and after the reused process. The XRD patterns show the crystals can be perfectly formed at M/L=1 : 1 in uniform octahedral shape. As the ratio of ligand reached 50%, the presence of an adequate amount of linkers caused an excellent condition to form the MOF nanocrystals [52,60-62]. According to the data obtained from the following figure, the location of peaks (orientation of parallel planes) at XRD patterns of MIL after repeatedly reproducing process is practically the same as the original sample. The only difference is related to the FWMH of these peaks that became wider after reusing process. This occurred due to the gradually deformation of MIL's framework in aqueous media and deviation from perfect well-grown octahedral crystals shape.

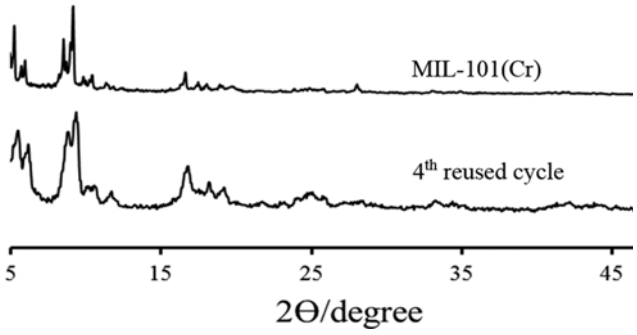

Fig. 5. The XRD pattern of materials.

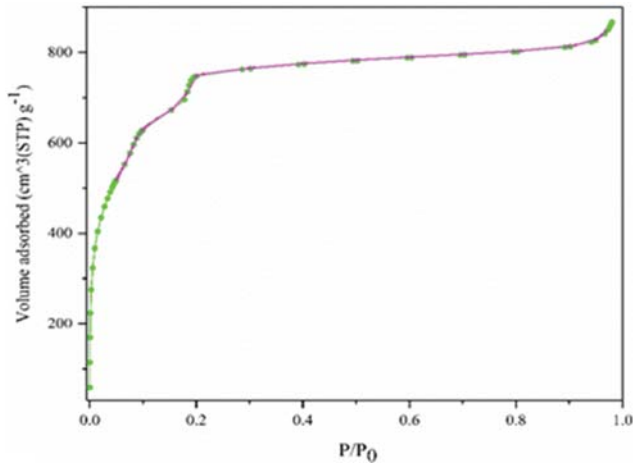

Fig. 6. N_2 adsorption-desorption analysis of MIL-101(Cr) with M/L=1 : 1.

The porosity and SSA of MIL were measured by adsorption and desorption of N_2 gas (Fig. 6). The SSA of the most effective adsorbent (MIL-101(Cr) with M/L=1 : 1) was 2,420 m^2/g. The large SSA verifies the high quality and precision of the water-based synthesized MIL-101(Cr) and leads to efficient adsorption of contaminants on the adsorbent surface.

The electrostatic attraction force between MIL surface charge and DR80 and AB92 molecules in aqueous solution is the most powerful driving force of the adsorption process. Herein, 0.015 g of MOF was added to 100 mL of distilled water at optimum pH value (pH=3), which led to maximum dye removal (%). The facts

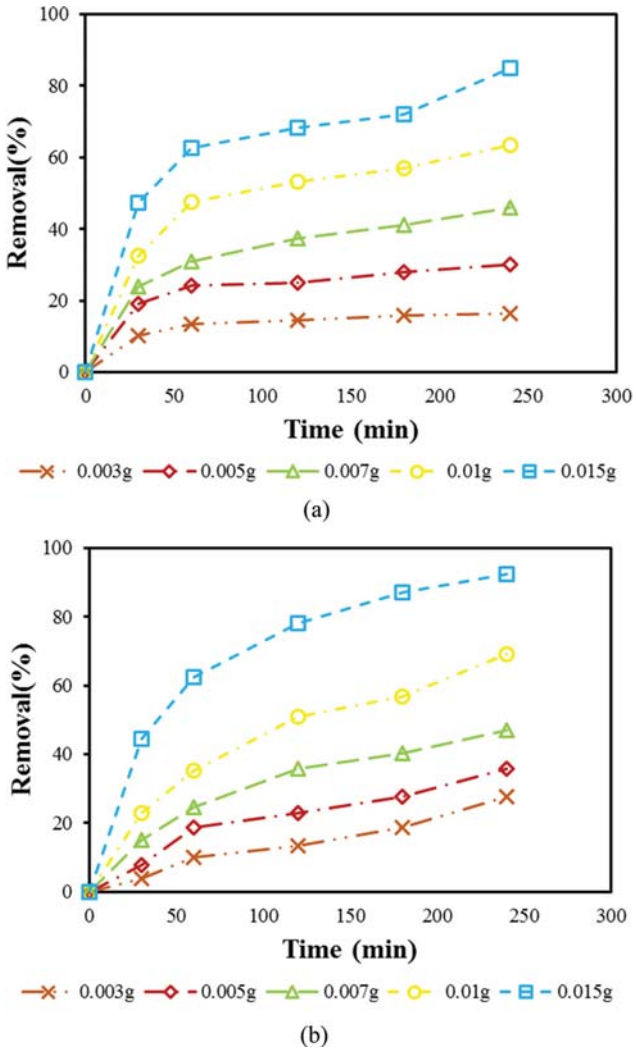

Fig. 7. The MIL dosage effect on removal (%) by the MIL-101 (Cr) at pH=3 and dye concentration=30 mg/L (a) AB 92 and (b) DR80.

show that the MIL-101(Cr) with M/L=1 : 1 has high positive surface charge (27.2 mV at pH=3). Therefore, the best adsorptive dye removal performance was obtained from a polar-polar attraction in MIL-101(Cr) with M/L=1 : 1 ratio.

2. The Operational Parameter Effects

The dye remediation performance of the synthesized MIL-101(Cr) was investigated by batch experiments. For this purpose, 100 mL of each dye solution at pH=3 and dye concentration of 30 mg/L was used to contact an attempt for studying the effect of the adsorbent dosage. At the end of each adsorption process, the suspension solid was filtered through high rpm centrifuging, and UV-Vis spectroscopy was used to test and record the final concentration of dye at every 30-min interval. The dye concentration study was done at the optimum dosage of MIL found in the previous section and constant pH=3. Finally, the effect of solution pH (3-10) was studied in acidic and basic range at the optimum dosage and optimum dye concentration.

In the present study, attempts were made to investigate the removal (%) of DR80 and AB92 by various dosages of MIL-101(Cr) at constant pH (3) and fix concentration (30 mg/L). Fig. 7 presents the removal (%) plots of DR80 and AB92 at different MIL dosages. According to the results, the removal (%) increased with increase in the amount of MIL dosage due to increase in the number of active spots.

0.015 g was chosen as the optimum dosage of M/L=1 : 1 in the removal process from dye solution. The obtained results depict increasing the amount of MOF loading led to an increment in removal (%). This can be due to the increase in the MIL-101(Cr) surface area and adsorption sites. The dye removal (%) obtained for DR80 and AB92 at 240 min was 92% and 85%, respectively.

In this work, the DR80 and AB92 concentration (30-60 mg/L) effect on removal (%) was studied at constant pH and the optimum dosage of MIL. The maximum removal (%) for AB92 and DR80 at the initial dye concentration of 30 mg/L achieved 85% and 92%, respectively (Fig. 8). Removal (%) was fast (contact time <60 min) at first but became slower over time.

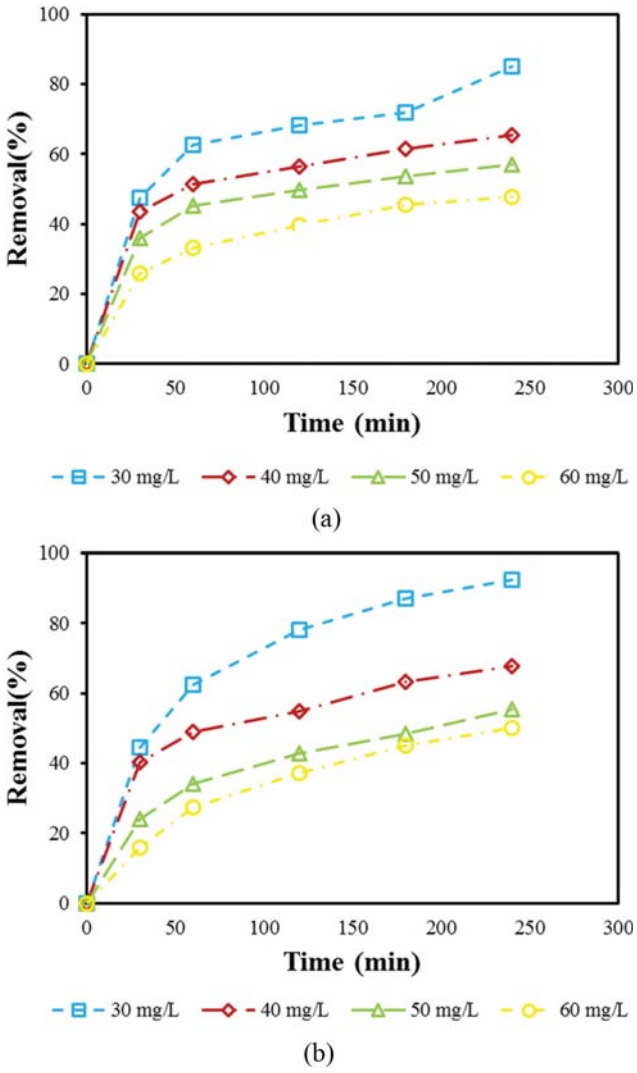

Fig. 8. Effect of dye concentration on removal (%) by the MIL-101(Cr) at pH=3 and the adsorbent dosage=0.15 g/L (a) DR80 and (b) AB92.

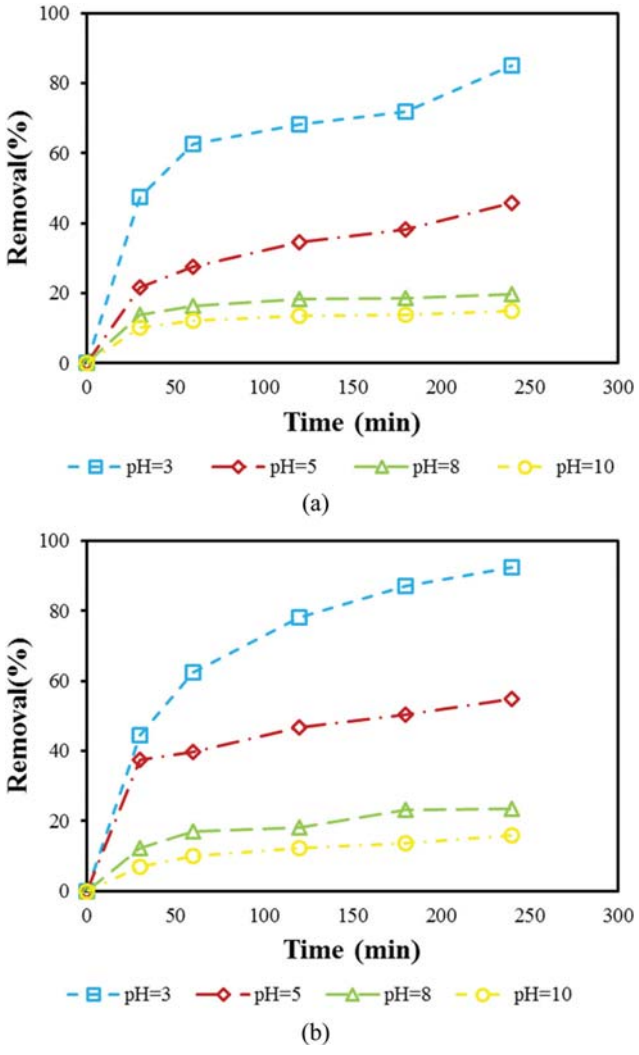

Fig. 9. Solution pH effect on removal (%) by MIL-101(Cr) at 30 mg/L of the solution and 0.015 g of adsorbent (a) AB92 and (b) DR80.

The solution pH is one of the significant and effective parameters in any adsorption process [63]. The tests were carried out at the optimum of the MIL dosage and dye concentration in the solution pH range of 3 to 10. Fig. 9 shows the effect of pH on the removal (%) of DR80 and AB92. The removal (%) of dye increases as well as the number of positively charged sites increase. Therefore, pH=3 as the optimum pH point was used for further studies.

To investigate the possible impact of linker on dye removal ability of the synthesized MIL, on the optimum point of adsorption process (pH=3, Concentration=30 mg/L, and Dosage=0.015 g), the dye adsorption behavior of H2BDC also was studied. The results show, the dye removal (%) for the both AB92 and DR80 was meas- ured and recorded at <0.5%. Therefore, a framework by itself (without metal) has no effect on the adsorption process (Fig. 10).

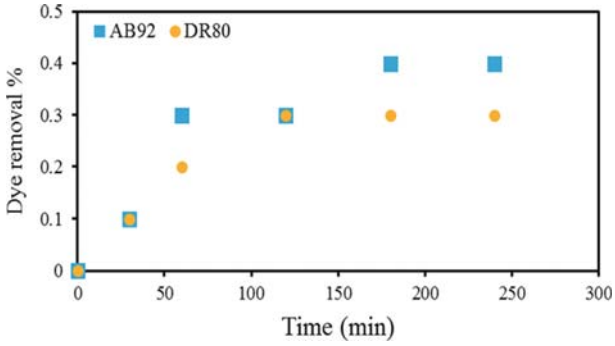

Fig. 10. AB92 and DR80 removal ability of H2BDC at the optimum point of the experiment.

3. RSM Modeling Construction

The removal percentages of two anionic dyes (AB92 and DR80) were studied by ANOVA as a statistical concept, to find the effect of the main involved factors and their interaction with dye adsorption. By considering the F value and P value for obtained significant models and non-significant lack of fit of models as the most important criteria of a practical model for dye removal behavior that presented at Table 1, following response surface methodology was finally applied for AB92 and DR80 removal (%) as the responses of model (R_{AB92} and R_{DR80}). The other statistical parameters of models such degree of freedom, the sum of squared, mean squared, coefficient of variation, adjusted and predicted R^2 were tabulated in Table 2.

$$\begin{aligned} R_{AB92} = {} & 36.3041 - 25.0339*pH + 6080.3*Dosage \\ & + 1.02909*Concentration + 0.208602*time \\ & - 0.0200695*pH*time + 8.60725*Dosage*time \\ & - 0.00205974*Concentration*time + 1.54495*pH^2 \\ & - 152448*Dosage^2 - 0.0194314*Concentration^2 \\ & - 0.000266362*time^2 \end{aligned} \quad (3)$$

$$\begin{aligned} R_{DR80} = {} & 86.4789 - 15.3902*pH + 3779.08*Dosage \\ & - 2.74378*Concentration + 0.340845*time \\ & - 0.0262201*pH*time + 6.80748*Dosage*time \\ & - 0.00217935*Concentration*time + 0.798914*pH^2 \\ & - 1679.29*Dosage^2 + 0.0206865*Concentration^2 \\ & - 0.000384529*time^2 \end{aligned} \quad (4)$$

Applicability of the presented models was validated by low P-value (<0.0001) and the closeness of the values of the predicted R^2 to the adjusted R^2 for both models. The amount of 0.0925 and 0.0513 of lack of fits (more than 0.05) refers to R_{DR80} and R_{AB92}, respectively, indicating the high quality of models.

4. 3D Plot Interpretation of Optimization Design

To get a better insight into each response (R_{AB92}, R_{DR80}), 3D surface plots of each pair of involved parameters were drawn and analyzed in the presence of the dye removal percentage. In these plots, as one pair of factors is representing, the two other parameters are kept fix.

Fig. 11 expresses that the efficiency of two anionic dyes removal

Table 1. ANOVA for reduced quadratic model for DR80 and AB92

Source	Sum of squares		df		Mean square		F-value		P-value		
	AB92	DR80	AB92	DR80	AB92	DR80	AB92	DR80	AB92	DR80	
Model	25047.29	28589.47	11	11	2277.03	2599.04	212.61	176.31	<0.0001	<0.0001	Significant
A-pH	10897.07	13560.91	1	1	10897.07	13560.91	1017.48	919.90	<0.0001	<0.0001	
B-Dosage	12067.44	12994.83	1	1	12067.44	12994.83	1126.76	881.50	<0.0001	<0.0001	
C-Concentration	1577.63	1043.08	1	1	1577.63	1043.08	147.31	70.76	<0.0001	<0.0001	
D-time	11.74	11.26	1	1	11.74	11.26	1.10	0.7637	0.3004	0.3865	
AD	522.13	891.20	1	1	522.13	891.20	48.75	60.45	<0.0001	<0.0001	
BD	340.88	213.23	1	1	340.88	213.23	31.83	14.46	<0.0001	0.0004	
CD	97.71	109.39	1	1	97.71	109.39	9.12	7.42	0.0040	0.0090	
A^2	1380.07	369.04	1	1	1380.07	369.04	128.86	25.03	<0.0001	<0.0001	
B^2	148.66	0.0180	1	1	148.66	0.0180	13.88	0.0012	0.0005	0.9722	
C^2	87.32	98.96	1	1	87.32	98.96	8.15	6.71	0.0063	0.0126	
D^2	84.84	176.81	1	1	84.84	176.81	7.92	11.99	0.0071	0.0011	
Residual	514.07	707.60	48	48	10.71	14.74					
Lack of fit	500.84	683.40	43	43	11.65	15.89	4.40	3.28	0.0513	0.0925	Not significant
Pure error	13.23	24.20	5	5	2.65	4.84					
Cor total	25561.36	29297.07	59	59							

Table 2. Statistical parameters of developed models

	AB92	DR80		AB92	DR80
Std. Dev.	3.27	3.84	R^2	0.9799	0.9758
Mean	39.44	38.48	Adjusted R^2	0.9753	0.9703
C.V. %	8.30	9.98	Predicted R^2	0.9686	0.9598

increases by passing the time and increasing the amount of adsorbent dosage. By increasing the amount of adsorbent dosage, the magnitude of active surface sites increased as the adsorptive specific area increased. Decreasing in adsorbent dosage caused higher ratio of dye molecules to active sites and lowest the dye removal percentage. Increasing in mixing time between adsorbent and dye let more opportunity to dye molecules so they could more adsorb on the adsorbent surface.

Dye concentration is one of driving force in the adsorption process. The rate of active site saturation increases by increasing the number of dye molecules collision on the adsorbent surface. As seen from Fig. 11(c) and Fig. 11(f), improvement in removal (%) occurred by concentrating the dye solution. Fig. 11(a) and 11(d) verify the solution pH by controlling the surface charge density of adsorbents particles made the important rule as the driving force of the adsorption process. The existence of this high positive charge is attributed to the functional group of the MIL-101(Cr) surface. Increasing the amount of dye removal at the lowest acidic pH values due to the more positive surface charge of adsorbent occurred.

5. Adsorption Isotherms and Kinetics

The Langmuir, Temkin, Freundlich, and Dubinin-Radushkevich equations were applied to find the mechanism of interaction between

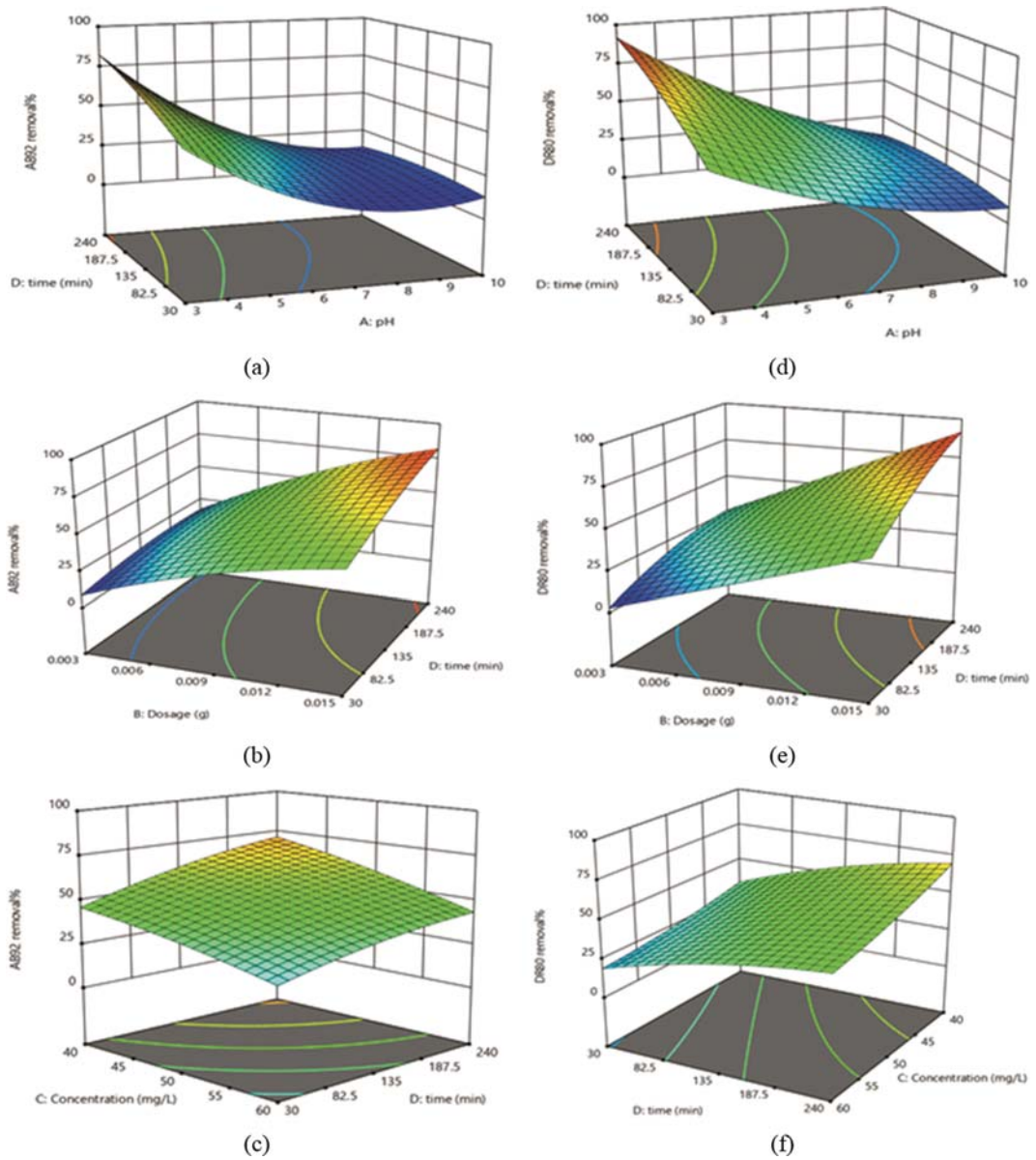

Fig. 11. 3D plots of parameters effect ((a), (b), and (c)) belong toAB92 and ((d), (e), and (f)) refer to DR80.

dye molecules and MIL surfaces. The isotherm models were studied at 100 mL of DR80 and AB92 solution at four concentrations (30, 40, 50, and 60 mg/L), 0.015 g of adsorbent dosage and optimum pH=3. After equilibrium, 2 mL of samples were pipetted out, centrifuged and UV-Vis spectroscopy was used to analyze them for the residual dye concentrations. At the end of the study process, the best model was chosen according to the higher R squared value.

The Langmuir isotherm model mainly deals with monolayer adsorption and homogeneity of adsorption sites and is used widely for the removal of pollutant from liquid solutions.

$$\frac{C_e}{q_e}=\frac{1}{q_{max}\times b}+\frac{C_e}{q_{max}} \quad (5)$$

It is possible to derive the q_{max} from the slope, which is denoted by $1/q_{max}$, and the value of b from the intercept, which is denoted by $1/(q_{max.}\ b)$ using the C_e/q_e versus C_e plot.

The Freundlich model studies the heterogeneous distribution of active sites. This model mainly describes the adsorption on the surfaces, where the adsorbed pollutant molecules interact with each other. This isotherm is denoted by the following linearized Eq. (6), which is used to describe the heterogeneous system:

$$\log q_e=\log K_F+\frac{1}{n}\log C_e \quad (6)$$

Therefore, the 1/n can be either irreversible (1/n=0), favorable (0< 1/n<1) or unfavorable (1/n>1).

According to the Temkin model (Eq. (7)), the interaction between adsorbate and adsorbent leads to a linear reduction in the adsorption heat generated by all molecules comprising a layer. This model also describes the adsorption process based on uniform distribution of binding energies.

$$q_e=\frac{RT}{b}\ln(K_tC_e)=B_1\ln(K_tC_e) \quad (7)$$

The study of adsorption mechanism on a porous, heterogeneous media with variable parameters is presented by the Dubinin-Radushkevich isotherm (Eq. (8)).

$$\ln q_e=\ln q_s-g\varepsilon^2 \quad (8)$$

where ε denotes the D-R isotherm constant and is represented as follows:

$$\varepsilon=RT\ln\left(1+\frac{1}{C_e}\right) \quad (9)$$

Table 3 shows the isotherm constants and the correlation coefficient (R^2) for the studied isotherm models. The results show that dye removal followed the Langmuir model due to the homogeneity of the adsorption surface on the MIL-101(Cr).

Four kinetic models including PFO (pseudo-first order), PSO (pseudo-second order), intraparticle diffusion, and the Elovich were studied to obtain the rate of dye adsorption. Suitable models can considerably contribute to a better understanding of the reaction of the process, analyzing the experimental data, and predicting purposes. The properties of the adsorbents and the mass transfer mechanism can affect the pollutant adsorption rate [64].

The PFO model can investigate the removal rate as adsorption proceeded on the solid surface through a boundary. This equation assumes that the adsorption process could be partially first-order and the contaminant concentration changes over time in proportion to the power one. The linear form of this equation is presented below:

$$\log(q_e-q_t)=\log(q_e)-\frac{tk_1}{2.303} \quad (10)$$

The log (q_e-q_t) versus t plots were applied to determine the values of k_1.

The Linear PSO model used in this work is as follows:

$$\frac{t}{q_t}=\frac{1}{k_2q_e^2}+\frac{t}{q_e} \quad (11)$$

The equilibrium sorption capacity (q_e) and the PSO rate constant (k_2) were calculated by the intercept and slope of the t/q_t versus t plot [65].

When the porosity of adsorbents affects adsorption mechanism, adsorption occurs by transportation of the adsorbate via intraparticle and film diffusion into porous media of solid phase and adsorption on the active sites:

$$q_t=k_pt^{1/2}+I \quad (12)$$

In this equation, the intraparticle rate constant ($g/mg\cdot min^{0.5}$) obtained from the slope of the plot is denoted by K_P.

The Elovich model can be expressed as follows [66]:

$$q_t=\beta\ln(\alpha\beta)+\beta\ln t \quad (13)$$

The slope and intercept of q_t versus Ln (t) plot are used to calculate the Elovich coefficients α and β, respectively.

According to Table 4, the PSO equation serves as a basis for the adsorption contaminations on the surface of the MOF. In this work, the PFO, PSO, intraparticle diffusion, and Elovich equations have studied the dye adsorption of MIL-101(Cr) 1 : 1 molar Cr^{3+} : H_2BDC ratio. According to results, the kinetic data had a better fit with the

Table 3. The isotherm data of dye adsorption by the MIL-101(Cr), M/L=1 : 1

Model	Parameters	Dyes	
		AB92	DR80
Langmuir	q_{max}	185.18	227.27
	b	18	0.22
	R^2	0.999	0.994
Freundlich	K_F	169.12	97.20
	n	33.44	4.80
	R^2	0.200	0.985
Temkin	B_1	5.1832	35.9340
	K_t	32.71	7.97
	R^2	0.180	0.973
Dubinin-Radushkevich	q_s	188.42	192.192
	g	0.394	2.88
	ε	1.126	0.417
	R^2	0.545	0.827

Table 4. The kinetic constants of dye removal by the synthesized MOF

Models and parameters		Dyes							
		AB92				DR80			
Concentration (mg/L)		30	40	50	60	30	40	50	60
PFO	$(q_e)_{cal.}$	124	141	176	155	203	230	282	310
	k_1	0.154	0.154	0.173	0.159	0.020	0.019	0.019	0.019
	R^2	0.983	0.951	0.968	0.974	0.949	0.856	0.828	0.809
PSO	$(q_e)_{cal.}$	20	78	22	22	22	23	26	27
	k_2	0.463	16.641	0.072	0.144	0.008	0.009	0.007	0.007
	R^2	0.970	0.966	0.976	0.969	0.971	0.957	0.948	0.940
Intraparticle diffusion	k_p	4.670	5.043	6.016	5.405	8.962	8.875	10.021	10.379
	I	100.93	120.51	95.08	103.61	18.93	32.11	29.97	37.34
	R^2	0.874	0.846	0.926	0.891	0.938	0.978	0.988	0.993
Elovich	α	1226.63	2131.8	77.43	69.55	5.89	8.17	8.22	9.82
	β	0.045	0.041	0.035	0.039	0.022	0.023	0.020	0.020
	R^2	0.906	0.878	0.952	0.915	0.987	0.995	0.991	0.977

PSO model compared to others.

5. Thermodynamic Study

To know the adsorption behavior of MIL at different temperature conditions, the experiments were carried out at the various temperatures (28, 35, and 50 °C). As can be seen in Fig. 12, the rise in the temperature causes the increase in adsorption capacity values. This observation validates the endothermic character of the adsorption of AB92 and DR80 onto MIL-101. The thermodynamic parameters change was studied for the determination of the thermodynamic behavior of adsorption process. The changes on the ther- modynamic parameters were calculated with the equations given below:

$$\Delta G^0 = -RT \ln K_d \quad (14)$$

$$K_d = \frac{q_e}{C_e} \quad (15)$$

$$\ln K_d = -\frac{\Delta H}{R}\left(\frac{1}{T}\right) + \frac{\Delta S}{R} \quad (16)$$

$$\Delta G^0 = (-T\Delta S^0 + \Delta H^0) \quad (17)$$

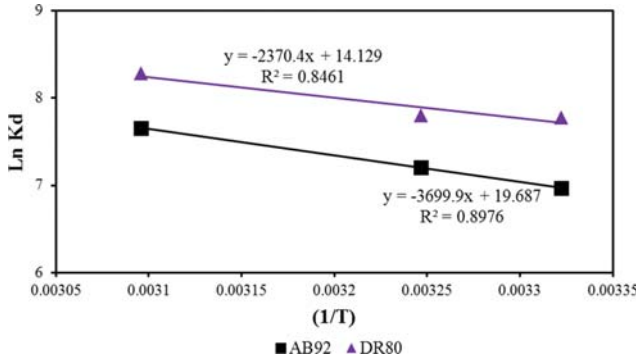

Fig. 12. Thermodynamic data of AB92 and DR80 adsorption on the MOF.

The positive value of entropy and enthalpy confirmed an endothermic adsorption process. The negative value of Gibbs free energy validates the spontaneous nature of adsorption. The negative value of ΔG, increases with rising temperature, suggesting approving adsorption at the higher temperature (Table 5) [67,68].

6. Dye Adsorption Mechanism

The common adsorption mechanisms (electrostatic interactions, hydrogen bonding, acid-base interactions, π-π interaction/stacking, pore shape/size selective adsorption and interactions with open metal sites) are usually proposed and studied in the water and wastewater purification process [38]. In this study, the π-π interaction between aromatic rings that contain π bonds refers to both adsorbents and adsorbate skeleton structures, and also strong electrostatic attraction between the positive surface charge of MIL-101(Cr) and negative charge of dye molecules, as a dipole-dipole force are the involved phenomenon of the adsorption process (Fig. 13).

According to the operational parameter effect, which was fully described in prior section, pH as the dominant mass transfer driving force, controls the pollutant remediation process (Fig. 9). At the high pH (basic range), although the SSA and pore volume of adsorbent had not changed, the adsorption capacity was decreased above 80%. In fact, however, the pollutant insertion into the crystal structure/pore of MOF, is one of the remediation mechanisms, but is not the main. Despite this, related to the Camille Petit [38] research, the obtained ΔH_{ads} in the range of (5-50 kJ·mol^{-1}) could validate that the main factor that controls the contaminant removal

Table 5. Thermodynamic data of AB92 and DR80 adsorption on the MIL

T (°C)	ΔG (kJ/mol)		ΔH (kJ/mol)		ΔS (J/mol)	
	AB92	DR80	AB92	DR80	AB92	DR80
28	−17.4	−19.3				
35	−18.4	−20.2	25.25	19.75	0.141	0.129
50	−20.5	−22.1				

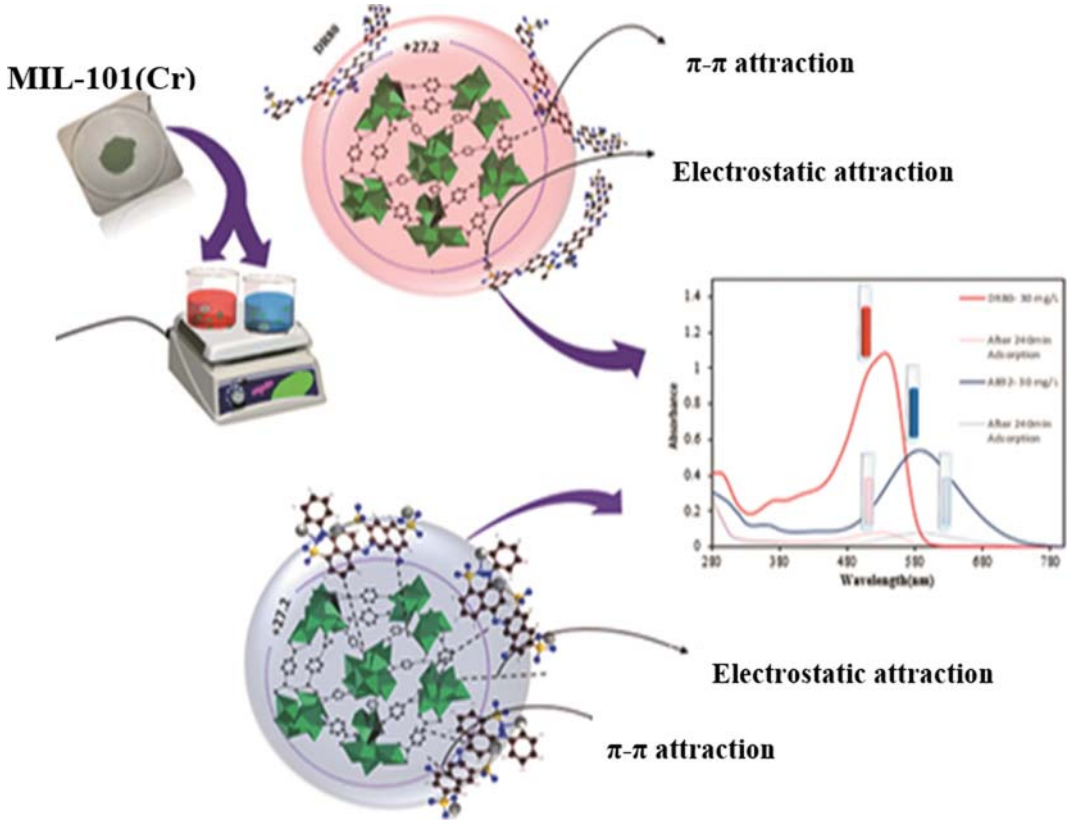

Fig. 13. The adsorption mechanism of AB92 on the MOF.

from wastewater is the physisorption aspect of adsorption phenomenon (Table 5).

7. Regeneration of MIL-101(Cr)

Regeneration and reusability of adsorbents are among the most challenging and significant parameters for the industrial and commercial feasibility of the adsorption process. The desorption process of AB92 and DR80 molecules loaded on MIL-101(Cr) was performed by 0.1 M HCl/ethanol (10 : 90, v/v) as an eluent and ultrasonic assistant. After four cycles, the adsorption capacity decreased ≤15% (Fig. 14). The results showed that the synthesized adsorbent had a high capacity for regeneration and reusability.

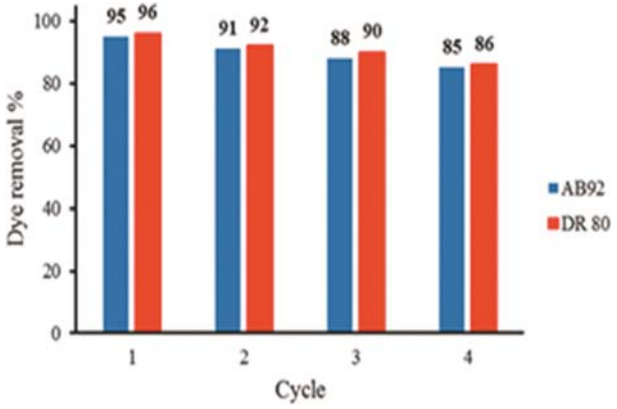

Fig. 14. The regeneration of MIL-101(Cr) as an adsorbent.

CONCLUSION

The nanoporous chromium-based metal-organic framework (MIL-101(Cr)) was ultrasound-assisted green synthesized and utilized for removing AB92 and DR80. Different analyses, such as FTIR, TGA, XRD, BET, SEM and Zeta potential, were applied and studied. The MIL-101(Cr) with the M/L=1 : 1 has with the BET surface area of 2,420 m^2/g and surface charge of 27.2 mV. The dataset of the adsorption process well matched with the PSO model (for AB92) and the PFO model (for DR80). The maximum adsorption capacity was obtained at 185 mg/g and 227 mg/g for AB92 and DR80, respectively. The synthesized MIL-101(Cr) could be considered as an alternative candidate for removing anionic dyes from the wastewater, and RSM was applied to the data to achieve an accurate model of the experiment. According to the data, the MIL-101(Cr) is suitable for the industrial application due to acceptable regeneration ability.

NOMENCLATURE

Alphabetic Letters

1/n : the constant corresponding to the surface heterogeneity
b : the Langmuir constant associated with the heat of adsorption [L/mg]
B1 : the heat of adsorption
BET : Brunauer-Emmett-Teller analysis
C_0 and C_e : the initial and equilibrium concentrations of dyes in

mg/L
FTIR : Fourier transform infrared
k_1 : the pseudo-first-order rate constant [1/min]
k_2 : the pseudo-second order rate constant [g/mg min]
K_F : the Freundlich constant corresponding to the adsorption capacity of the adsorbent [mg/g]
k_p : intraparticle rate constant [g/mg·min$^{0.5}$]
K_t : the equilibrium binding constant (L/mg) corresponding to the maximum binding energy
m : the mass of the adsorbent used in mg
q_e : the amount of pollutant adsorbed on adsorbent (mg/g) at equilibrium
q_{max} : the maximum capacity of adsorbate used to form a complete monolayer on the surface [mg/g]
q_t : the amount of dye adsorbed on adsorbent at a time t
R^2 : the correlation coefficient
SEM : scanning electron microscopy
V : the volume of dye solution in mL
XRD : X-ray diffraction
q_s : the theoretical isotherm adsorption capacity [mg/g]
g : D-R isotherm constant [mol^2/kJ^2]
R : the gas constant [8.314 J/mol K]
T : temperature [K]

Greek Letters

α : the initial dye adsorption rate [mg/g min]
β : the desorption constant corresponding to the surface coverage and the chemisorption (g/mg) activation energy
ε : the D-R isotherm constant

REFERENCES

1. N. M. Mahmoodi, M. Arabloo, and J. Abdi, *Water Res.*, **67**, 216 (2014).
2. N. M. Mahmoodi, *Prog. Color Colorants Coat.*, **9**, 161 (2016).
3. N. M. Mahmoodi, *J. Environ. Eng.*, **139**, 1368 (2013).
4. N. M. Mahmoodi, M. Arami, N. Y. Limaee, K. Gharanjig, and F. Nourmohammadian, *Mater. Res. Bull.*, **42**, 797 (2007).
5. N. M. Mahmoodi and M. Arami, *Chem. Eng. J.*, **146**, 189 (2009).
6. G. Bayramoglu and M. Y. Arica, *Korean J. Chem. Eng.*, **35**, 1303 (2018).
7. Y. Wang, T. Du, L. Zhou, Y. Song, S. Che and X. Fang, *Korean J. Chem. Eng.*, **35**, 709 (2018).
8. S. Wang and Z. H. Zhu, *J. Hazard. Mater.*, **136**, 946 (2006).
9. K. R. Ramakrishna and T. Viraraghavan, *Water Sci. Technol.*, **36**, 189 (1997).
10. T. Calvete, E. C. Lima, N. F. Cardoso, J. C. P. Vaghetti, S. L. P. Dias and F. A. Pavan, *J. Environ. Manage.*, **91**, 1695 (2010).
11. M. Hartmann, S. Kunz, D. Himsl, O. Tangermann, S. Ernst and A. Wagener, *Langmuir*, **24**, 8634 (2008).
12. I. U. Haq, H. N. Bhatti and M. Asgher, *Can. J. Chem. Eng.*, **89**, 593 (2011).
13. N. N. Bahrudin, M. A. Nawi and W. I. N. W. Ismail, *Korean J. Chem. Eng.*, **35**, 1450 (2018).
14. A. Mittal, A. Malviya, D. Kaur, J. Mittal and L. Kurup, *J. Hazard. Mater.*, **148**, 229 (2007).
15. S. Chen, J. Zhang, C. Zhang, Q. Yue, Y. Li and C. Li, *Desalination*, **252**, 149 (2010).
16. N. M. Mahmoodi, *J. Ind. Eng. Chem.*, **20**, 2050 (2014).
17. F. Momtazan, A. Vafaei, M. Ghaedi, A. M. Ghaedi, D. Emadzadeh, W.-J. Lau and M. M. Baneshi, *Korean J. Chem. Eng.*, **35**, 1108 (2018).
18. V. Gupta, I. Ali, Suhas and D. Mohan, *J. Colloid Interface Sci.*, **265**, 257 (2003).
19. F. A. Pavan, S. L. P. Dias, E. C. Lima and E. V. Benvenutti, *Dye. Pigment.*, **76**, 64 (2008).
20. V. K. Gupta, D. Mohan and V. K. Saini, *J. Colloid Interface Sci.*, **298**, 79 (2006).
21. A. Sarı and M. Tuzen, *J. Hazard. Mater.*, **160**, 349 (2008).
22. R. A. Anayurt, A. Sari and M. Tuzen, *Chem. Eng. J.*, **151**, 255 (2009).
23. A. Sarı and M. Tuzen, *J. Hazard. Mater.*, **152**, 302 (2008).
24. R. J. Kuppler, D. J. Timmons, Q.-R. Fang, J.-R. Li, T. A. Makal, M. D. Young, D. Yuan, D. Zhao, W. Zhuang and H.-C. Zhou, *Coord. Chem. Rev.*, **253**, 3042 (2009).
25. P. Rocío-Bautista, C. Martínez-Benito, V. Pino, J. Pasán, J. H. Ayala, C. Ruiz-Pérez and A. M. Afonso, *Talanta*, **139**, 13 (2015).
26. J. Abdi, M. Vossoughi, N. M. Mahmoodi, and I. Alemzadeh, *Chem. Eng. J.,* **326**, 1145 (2017).
27. Q. Zhu, Y. Chen, W. Wang, H. Zhang, C. Ren, H. Chen and X. Chen, *Sensors Actuators B Chem.*, **210**, 500 (2015).
28. M. Oveisi, M. A. Asli, and N. M. Mahmoodi, *J. Hazard. Mater.,* **347**, 123 (2018).
29. N. M. Mahmoodi, J. Abdi, M. Oveisi, M. A. Asli, and M. Vossoughi, *Mater. Res. Bull.,* **100**, 357 (2018).
30. H.-M. Jeong, R. Roshan, R. Babu, H.-J. Kim and D.-W. Park, *Korean J. Chem. Eng.*, **35**, 438 (2018).
31. Y.-R. Lee, S.-M. Cho and W.-S. Ahn, *Korean J. Chem. Eng.*, **35**, 1542 (2018).
32. S. Bae, N. Zaini, K. S. N. Kamarudin, K. S. Yoo, J. Kim and M. R. Othman, *Korean J. Chem. Eng.*, **35**, 764 (2018).
33. M. Hartmann and M. Fischer, *Micropor. Mesopor. Mater.*, **164**, 38 (2012).
34. M. Wickenheisser, A. Herbst, R. Tannert, B. Milow and C. Janiak, *Micropor. Mesopor. Mater.*, **215**, 143 (2015).
35. J. R. Long and O. M. Yaghi, *Chem. Soc. Rev.*, **38**, 1213 (2009).
36. H. Li, M. Eddaoudi, M. O'Keeffe, and O. M. Yaghi, *Nature*, **402**, 276 (1999).
37. M. Eddaoudi, D. F. Sava, J. F. Eubank, K. Adil, and V. Guillerm, *Chem. Soc. Rev.,* **44**, 228 (2015).
38. C. Petit, *Curr. Opin. Chem. Eng.*, **20**, 132 (2018).
39. N. Al-Janabi, P. Hill, L. Torrente-Murciano, A. Garforth, P. Gorgojo, F. Siperstein and X. Fan, *Chem. Eng. J.*, **281**, 669 (2015).
40. W. Zhang, O. Kozachuk, R. Medishetty, A. Schneemann, R. Wagner, K. Khaletskaya, K. Epp and R. A. Fischer, *Eur. J. Inorg. Chem.*, **2015**, 3913 (2015).
41. F. Wang, H. Guo, Y. Chai, Y. Li and C. Liu, *Micropor. Mesopor. Mater.*, **173**, 181 (2013).
42. G. Férey, *Chem. Soc. Rev.*, **37**, 191 (2008).
43. S. Kitagawa, R. Kitaura and S. Noro, *Angew. Chemie Int. Ed.*, **43**, 2334 (2004).
44. O. M. Yaghi, M. O'Keeffe, N. W. Ockwig, H. K. Chae, M. Eddaoudi and J. Kim, *Nature*, **423**, 705 (2003).

45. I. J. Kang, N. A. Khan, E. Haque and S. H. Jhung, *Chem. - A Eur. J.*, **17**, 6437 (2011).
46. D. K. Panchariya, R. K. Rai, S. K. Singh and E. A. Kumar, *Mater. Today Proc.*, **4**, 388 (2017).
47. G. Férey, C. Mellot-Draznieks, C. Serre, F. Millange, J. Dutour, S. Surblé and I. Margiolaki, *Science*, **309**, 2040 (2005).
48. B. Chen, N. W. Ockwig, A. R. Millward, D. S. Contreras and O. M. Yaghi, *Angew. Chem.*, **117**, 4823 (2005).
49. Y. K. Hwang, D.-Y. Hong, J.-S. Chang, S. H. Jhung, Y.-K. Seo, J. Kim, A. Vimont, M. Daturi, C. Serre and G. Férey, *Angew. Chem. Int. Ed.*, **47**, 4144 (2008).
50. D. Y. Hong, Y. K. Hwang, C. Serre, G. Férey and J. S. Chang, *Adv. Funct. Mater.*, **19**, 1537 (2009).
51. M. Arami, N. Y. Limaee, N. M. Mahmoodi and N. S. Tabrizi, *J. Hazard. Mater.*, **135**, 171 (2006).
52. Y.-F. Huang, M. Liu, Y.-Q. Wang, Y. Li, J.-M. Zhang and S.-H. Huo, *RSC Adv.*, **6**, 15362 (2016).
53. M. Ghaedi, A. M. Ghaedi, E. Negintaji, A. Ansari, A. Vafaei and M. Rajabi, *J. Ind. Eng. Chem.*, **20**, 1793 (2014).
54. M. Naushad, G. Sharma, A. Kumar, S. Sharma, A. A. Ghfar, A. Bhatnagar, F. J. Stadler and M. R. Khan, *Int. J. Biol. Macromol.*, **106**, 1 (2018).
55. Z. J. Sun, Z. W. Jiang and Y. F. Li, *RSC Adv.*, **6**, 79805 (2016).
56. Z. Zhang, H. Wang, X. Chen, C. Zhu, W. Wei and Y. Sun, *Adsorption*, **21**, 77 (2015).
57. Z. Yu, J. Deschamps, L. Hamon, P. Karikkethu Prabhakaran and P. Pre, *Int. J. Hydrogen Energy*, **42**, 8021 (2017).
58. S. Kayal and A. Chakraborty, *Chem. Eng. J.*, **334**, 780 (2018).
59. S. M. Mirsoleimani-azizi, P. Setoodeh, F. Samimi, J. Shadmehr, N. Hamedi and M. R. Rahimpour, *J. Environ. Chem. Eng.*, **6**, 4653 (2018).
60. Z. Zhou, B. Cheng, C. Ma, F. Xu, J. Xiao, Q. Xia and Z. Li, *RSC Adv.*, **5**, 94276 (2015).
61. S. Xian, Y. Yu, J. Xiao, Z. Zhang, Q. Xia, H. Wang and Z. Li, *RSC Adv.*, **5**, 1827 (2015).
62. J. Kim, Y.-R. Lee and W.-S. Ahn, *Chem. Commun.*, **49**, 7647 (2013).
63. N. Ballav, A. Maity and S. B. Mishra, *Chem. Eng. J.*, **198-199**, 536 (2012).
64. E. Alver and A. U. Metin, *Chem. Eng. J.*, **200-202**, 59 (2012).
65. A. Kausar, H. N. Bhatti and G. MacKinnon, *J. Taiwan Inst. Chem. Eng.*, **59**, 330 (2016).
66. S. Ben-Ali, I. Jaouali, S. Souissi-Najar and A. Ouederni, *J. Clean. Prod.*, **142**, 3809 (2017).
67. N. M. Mahmoodi, M. Taghizadeh and A. Taghizadeh, *J. Mol. Liq.*, **269**, 217 (2018).
68. D. C. dos Santos, M. A. Adebayo, S. de Fátima Pinheiro Pereira, L. D. T. Prola, R. Cataluña, E. C. Lima, C. Saucier, C. R. Gally and F. M. Machado, *Korean J. Chem. Eng.*, **31**, 1470 (2014).